

Non-local thermal transport via molecular-dynamics simulation and the Green-Kubo formalism

Kevin Fernando^a, Patrick K. Schelling^{a,b,*}

^a*Department of Physics, University of Central Florida, Orlando, FL 32816-2385, USA*

^b*Advanced Materials Processing and Analysis Center, University of Central Florida, Orlando, FL 32804, USA*

Abstract

In this article we develop the theory of nonlocal thermal transport within the context of the fluctuation-dissipation theorem. The theory goes beyond the usual Green-Kubo integrals used to obtain the thermal conductivity by including the response of a system to external heat sources that are nonuniform in space and time. Through the integration of current-current correlation functions, the relevant response functions are determined from equilibrium molecular-dynamics simulations of an Ar crystal modeled using the standard Lennard-Jones potential. It is shown that for low temperatures and short length scales, the approach can be used to elucidate partially-ballistic transport. Transport can be understood to be heat waves in the sense that transport is primarily limited by the sound velocity. By contrast, at longer length scales and higher temperatures, the response functions become more comparable to what is expected from Fourier's law where diffusive heat transport is the dominant mechanism. It is also shown how the effective thermal conductivity can be determined in a partially-ballistic regime. The results demonstrate the known reduction in the effective thermal conductivity seen in the partially-ballistic regime. Finally, we show how determination of the relevant response functions can be used to model heating of a crystal without requiring additional atomic-scale simulations. This approach is used to show how temperature profiles differ from those expected from the diffusive Fourier's law due to nonlocal transport effects.

1. Introduction

Thermal conduction is most often described using Fourier's law. Specifically, the Cartesian components of the heat-flux density \vec{J} are related to the temperature gradient $\vec{\nabla}T$ using,

$$J_\mu = - \sum_\nu \kappa_{\mu\nu} \frac{\partial T}{\partial x_\nu} \quad (1)$$

in which J_μ is a component of the heat-flux density, x_ν is a component of the position vector \vec{x} , and $\kappa_{\mu\nu}$ is an element of the thermal conductivity tensor. An important assumption of Eq. 1 is that the heat-flux density depends only on the local temperature gradient at a single instant of time. An important requirement for Eq. 1 to apply is that the separation between any heat sources and sinks be large enough that transport

*Corresponding author.

Email address: `patrick.schelling@ucf.edu` (Patrick K. Schelling)

is diffusive. In many instances this is a good assumption, but in nanoscale devices this may not be the case [1, 2]. Specifically, if the separation between a heat source and sink is comparable or less than the mean-free path Λ of heat carriers, then transport will be at least partially ballistic and Eq. 1 will not exactly apply. Moreover, when the heat sources and sinks depend on time, heat transport should be limited by the group velocity of phonon waves. This feature, which is relevant primarily for ballistic transport, is not captured by Fourier’s law.

Partially-ballistic transport can be directly observed in “direct” molecular-dynamics (MD) simulations which use a heat source and sink and Fourier’s law to obtain the effective thermal conductivity. Specifically, it was shown in Ref. [3] that MD simulation yields a linear dependency of $\frac{1}{\kappa}$ on $\frac{1}{L}$ where L is the separation between the heat source and sink. Over the past several years, improved insight and more accurate calculations have demonstrated that the linear dependence assumed in Ref. [3] is overly simplistic. This is now understood to be due to the fact that scattering rates of vibrational modes depend rather strongly on wavelength [4]. Partially-ballistic transport also results in nonlinear temperature profiles [5]. In Ref. [5] a nonlocal theory for thermal conduction was developed to probe partially-ballistic effects. Specifically, a non-local response function $\kappa(\vec{x}, \vec{x}')$ was used to relate the temperature profile in an MD calculation to the heat-current density via the expression,

$$J_{\mu}(\vec{x}, t) = - \int \kappa(\vec{x}, \vec{x}') \frac{\partial T(\vec{x}')}{\partial x'_{\mu}} d^3 x' \quad (2)$$

This theory was used in reciprocal space to describe results of extensive MD calculations using the direct method for conduction in GaN [6], with the assumption that for an ideal periodic system $\kappa(\vec{x}, \vec{x}') = \kappa(\vec{x} - \vec{x}')$, the Fourier-transformed response $\tilde{\kappa}(\vec{k})$ was directly obtained. The dependence $\tilde{\kappa}(\vec{k})$ on the magnitude $|\vec{k}|$ was interpreted by solving the Peierls-Boltzmann Equation (PBE) with different models for the dependence of scattering time on phonon wave vector. Solutions were obtained within the relaxation-time approximation (RTA) and very good agreement with MD results was demonstrated [5]. An important result of this approach was that insight into how scattering rates depend on phonon wave vector was obtained. Moreover, the approach developed in Ref. [5] demonstrates a way to extract and understand nanoscale transport effects from an MD simulation.

Another simulation approach for obtaining thermal transport properties is to use equilibrium MD simulation and the Green-Kubo (GK) formulation of the fluctuation-dissipation theorem [7, 8]. Specifically, the thermal conductivity of a system in equilibrium at temperature T can be computed using,

$$\kappa_{\mu\nu} = \frac{\Omega}{k_B T^2} \int_0^{\infty} \langle J_{\mu}(\tau) J_{\nu}(0) \rangle d\tau \quad (3)$$

in which Ω is the system volume and k_B is the Boltzmann constant. Generally, predictions for κ obtained with Eq. 3 do not agree with direct-method calculations due to partially-ballistic transport in the latter case. Hence, it is generally believed that the Green-Kubo approach is more appropriate for determining bulk transport properties. To the best of our knowledge, Green-Kubo methods have not previously been used to extract nonlocal transport properties.

The theory of nonlocal thermal conductivity was first developed in Ref. [9]. In this paper, we consider a general nonlocal form with response function $K_{\mu\nu}(\vec{x} - \vec{x}', t - t')$, which relates the heat flux density to the external heat sources and sinks,

$$J_{\mu}(\vec{x}, t) = -\frac{1}{C_p} \int_{\Omega} \int_{-\infty}^t \sum_{\nu} K_{\mu\nu}(\vec{x} - \vec{x}', t - t') \frac{\partial^2 \Delta h^{(ext)}(\vec{x}', t')}{\partial t' \partial x'_{\nu}} d^3 x' dt' \quad (4)$$

in which $\Delta h^{(ext)}(\vec{x}', t')$ represents the heat density, specifically the enthalpy density, added or removed locally near \vec{x}' and C_p is constant-pressure heat capacity the atoms within the volume Ω . This expression takes into account the finite propagation time for the heat pulse, and hence an important limitation on ballistic transport. While this expression is suitable for time-dependent heat sources and sinks, it can also be applied to static nonequilibrium situations. Hence this is compatible with the expression in Eq. 2, but goes somewhat beyond it to time-dependent situations which would be relevant to many experiments including pulsed laser heating or the response of materials to high-frequency heating via electron-phonon scattering in semiconductor devices. We develop an approach to use Green-Kubo calculations to determine the nonlocal response function, which is then applied to transport in a periodic Lennard-Jones solid. This work suggests a way forward for using Green-Kubo simulations to generate predictions that are applicable at the nanoscale where Fourier's law breaks down.

2. Green-Kubo expressions for non-local heat transport

In this section we develop the expression for nonlocal thermal transport that can be used in an equilibrium MD simulation. We begin with a representation of the important quantities in reciprocal space which is relevant for a bulk periodic solid. First, the heat-current density can be written as a Fourier series,

$$J_{\mu}(\vec{x}, t) = \tilde{J}_{\mu}(0, t) + \sum_{\vec{k} \neq 0} \tilde{J}_{\mu}(\vec{k}, t) e^{i\vec{k} \cdot \vec{x}} \quad (5)$$

The action of heat sources and sinks is represented by the enthalpy-density function $\Delta h^{(ext)}(\vec{x}', t')$, which can be expanded in a Fourier series,

$$\Delta h^{(ext)}(\vec{x}', t') = \sum_{\vec{k} \neq 0} \tilde{h}^{(ext)}(\vec{k}, t') e^{i\vec{k} \cdot \vec{x}'} \quad (6)$$

in which we have made the assumption that the net input enthalpy is zero, hence $\tilde{h}(\vec{k} = 0, t') = 0$ at all times. The response function is similarly expanded, with the assumption that the system in question is periodic,

$$K_{\mu\nu}(\vec{x} - \vec{x}', t - t') = \tilde{K}_{\mu\nu}(0, t - t') + \sum_{\vec{k} \neq 0} \tilde{K}_{\mu\nu}(\vec{k}, t - t') e^{i\vec{k} \cdot (\vec{x} - \vec{x}')} \quad (7)$$

Substitution of these expressions into Eq. 4 yields,

$$\tilde{J}_{\mu}(\vec{k}, t) = -i \frac{\Omega}{C_p} \sum_{\nu} \int_{-\infty}^t k_{\nu} \tilde{K}_{\mu\nu}(\vec{k}, t - t') \frac{\partial \tilde{h}^{(ext)}(\vec{k}, t')}{\partial t'} dt' \quad (8)$$

To obtain an expression which can be used to evaluate the response functions, we consider an external source,

$$\frac{\partial \tilde{h}^{(ext)}(\vec{k}, t')}{\partial t'} = \tilde{h}^{(ext)}(\vec{k}) \delta(t') \quad (9)$$

in which $\delta(t')$ is the Dirac delta function. Using Eq. 9 the integral in Eq. 8 can be evaluated,

$$\tilde{J}_\mu(\vec{k}, t) = -i \frac{\Omega}{C_p} \sum_\nu k_\nu \tilde{K}_{\mu\nu}(\vec{k}, t) \tilde{h}^{(ext)}(\vec{k}) \quad (10)$$

This expression determines the heat-flux density which results from an input energy. It is moreover understood that the response function $\tilde{K}_{\mu\nu}(\vec{k}, t)$ is zero for $t < 0$.

To obtain the response function, we can develop a Green-Kubo expression starting from Eq. 10. First we assume that an external source $\tilde{h}^{(ext)}(\vec{k})$ can be equated to a fluctuation of a system in equilibrium $\tilde{h}(\vec{k})$. After this substitution, we multiply Eq. 10 by $ik_\mu \tilde{h}(-\vec{k})$, sum over each direction μ , and take an ensemble average,

$$\sum_\mu \langle ik_\mu \tilde{J}_\mu(\vec{k}, \tau) \tilde{h}(-\vec{k}) \rangle = \frac{\Omega}{C_p} \sum_\mu \sum_\nu k_\mu k_\nu \tilde{K}_{\mu\nu}(\vec{k}, \tau) \langle \tilde{h}(\vec{k}) \tilde{h}(-\vec{k}) \rangle \quad (11)$$

where τ is the time relative to the fluctuation. Using the continuity equation and time-reversal symmetry, and finally taking a derivative with respect to τ , it can then be shown that the response function is given by,

$$\frac{\partial \tilde{K}_{\mu\nu}(\vec{k}, \tau)}{\partial \tau} = \left(\frac{C_p}{\Omega} \right) \frac{\langle \tilde{J}_\mu(\vec{k}, \tau) \tilde{J}_\nu(-\vec{k}, 0) \rangle}{\langle \tilde{h}(\vec{k}) \tilde{h}(-\vec{k}) \rangle} \quad (12)$$

Integration of this expression over the time variable τ results in,

$$\tilde{K}_{\mu\nu}(\vec{k}, \tau) - \tilde{K}_{\mu\nu}(\vec{k}, 0) = \left(\frac{C_p}{\Omega} \right) \frac{\int_0^\tau \langle \tilde{J}_\mu(\vec{k}, \tau') \tilde{J}_\nu(-\vec{k}, 0) \rangle d\tau'}{\langle \tilde{h}(\vec{k}) \tilde{h}(-\vec{k}) \rangle} \quad (13)$$

Next we use the fluctuation formula for the heat capacity,

$$\langle \tilde{h}(\vec{k}) \tilde{h}(-\vec{k}) \rangle = \frac{C_p k_B T^2}{\Omega^2} \quad (14)$$

From this we obtain,

$$\tilde{K}_{\mu\nu}(\vec{k}, \tau) - \tilde{K}_{\mu\nu}(\vec{k}, 0) = \frac{\Omega}{k_B T^2} \int_0^\tau \langle \tilde{J}_\mu(\vec{k}, \tau') \tilde{J}_\nu(-\vec{k}, 0) \rangle d\tau' \quad (15)$$

It is evident that the response function should vanish in the limit $\tau \rightarrow \infty$, hence we have

$$\tilde{K}_{\mu\nu}(\vec{k}, 0) = -\frac{\Omega}{k_B T^2} \int_0^\infty \langle \tilde{J}_\mu(\vec{k}, \tau') \tilde{J}_\nu(-\vec{k}, 0) \rangle d\tau' \quad (16)$$

However, for finite \vec{k} values (i.e. $\vec{k} \neq 0$) this integral should also vanish. This is clear because if the integral on the right-hand-side of Eq. 16 were to not vanish, the system would tend towards a non-equilibrium distribution of energy. Instead, we require that $\langle \tilde{h}(\vec{k}) \rangle = 0$ for $\vec{k} \neq 0$, with the result that the integral in Eq. 16 vanishes and hence $\tilde{K}_{\mu\nu}(\vec{k}, 0) = 0$. It will be shown that the computational results support this condition on the response function. Finally then, the response function for $\tau \geq 0$ is given simply by,

$$\tilde{K}_{\mu\nu}(\vec{k}, \tau) = \frac{\Omega}{k_B T^2} \int_0^\tau \langle \tilde{J}_\mu(\vec{k}, \tau') \tilde{J}_\nu(-\vec{k}, 0) \rangle d\tau' \quad (17)$$

whereas $\tilde{K}_{\mu\nu}(\vec{k}, \tau) = 0$ for $\tau \leq 0$. In the following we consider a system with cubic symmetry, such that

$$\tilde{K}_{\mu\nu}(\vec{k}, \tau) = \tilde{K}(\vec{k}, \tau)\delta_{\mu,\nu} \quad (18)$$

where $\delta_{\mu,\nu}$ is the Kroenecker delta function. In this case the current direction is exactly along the direction \vec{k} corresponding to the external perturbation. Hence we can define,

$$\tilde{J}_\mu(\vec{k}, \tau) = \tilde{J}(\vec{k}, \tau)\frac{k_\mu}{k} \quad (19)$$

in which $k = |\vec{k}|$. Given these simplifications for a cubic system, it is then easy to show that the response function only depends on the magnitude of \vec{k} . We obtain the expression,

$$\tilde{K}(\vec{k}, \tau) = \frac{\Omega}{k_B T^2} \int_0^\tau \langle \tilde{J}(\vec{k}, \tau') \tilde{J}(-\vec{k}, 0) \rangle d\tau' \quad (20)$$

Moreover, the connection between the response function in the limit $k \rightarrow 0$ and the usual Green-Kubo expression for the thermal conductivity in Eq. 3 is quite clear.

To compare to Fourier's law and obtain direct insight into the non-local wave nature of the transport, we report the Fourier transform of the function $\tilde{K}(\vec{k}, \tau)$,

$$\tilde{K}_T(\vec{k}, \omega) = \int_0^\infty \tilde{K}(\vec{k}, \tau) e^{-i\omega\tau} d\tau \quad (21)$$

The choice of the integration limits accounts for the fact that the response is causal, and as previously noted that response function vanishes for $\tau \leq 0$. Finally, it should be noted that $\tilde{K}(\vec{k}, \tau)$ is real, and hence $\tilde{K}(\vec{k}, \tau) = \tilde{K}(-\vec{k}, \tau)$. It then follows that $\tilde{K}_T(\vec{k}, \omega)$ is complex and should satisfy the relation $\tilde{K}_T^*(\vec{k}, \omega) = \tilde{K}_T(\vec{k}, -\omega)$.

3. Computational approach

The simulation results were obtained using a Lennard-Jones (LJ) solid in an fcc lattice. Periodic-boundary conditions were applied in all three directions. Although the results could be given in terms of reduced units, we used LJ parameters applicable to the model for LJ argon. The pair-potential was determined from,

$$u(r) = 4\epsilon \left[\left(\frac{\sigma}{r}\right)^{12} - \left(\frac{\sigma}{r}\right)^6 \right] \quad (22)$$

For the LJ parameters, we took $\sigma = 3.40\text{\AA}$, and $\epsilon = \frac{120K}{k_B}$. A smooth cutoff at a distance $r = 3\sigma$ was used. Specifically, the pair potential $u_{mod}(r)$ given by,

$$u_{mod}(r) = u(r) - u(r = r_c) - \left[\frac{du}{dr} \right]_{r=r_c} (r - r_c) \quad (23)$$

was used in the calculations for $r \leq r_c$. For $r > r_c$, the pair potential is taken to be zero. It is easily seen that the above expression yields $u_{mod}(r = r_c) = 0$, and moreover the force obtained is also zero at $r = r_c$. Finally, the atomic mass was taken to be $m = 39.948$ in atomic-mass units.

The heat-flux density is defined using the standard expression relevant for a pair potential (e.g. see Ref. [3]). Here we distinguish the contribution to the heat-flux density assigned locally to a specific atom. Specifically, we define a component of the heat-flux density associated with atom i as,

$$J_{i,\mu}(t) = \frac{1}{\Omega} \left[v_{i,\mu} (\epsilon_i - \langle h \rangle) + \frac{1}{2} \sum_{j \neq i} r_{ij,\mu} \left(\vec{F}_{ij} \cdot \vec{v}_i \right) \right] \quad (24)$$

in which $v_{i,\mu}$ is the μ th component of the velocity \vec{v}_i , $r_{ij,\mu}$ is the μ th component of the vector $\vec{r}_{ij} = \vec{r}_i - \vec{r}_j$, and \vec{F}_{ij} is the pairwise force due to the interaction between atoms i and j . The energy ϵ_i is the sum of the potential and kinetic energies, with the potential energy for each pair evenly divided between the two atoms [3]. The quantity $\langle h \rangle$ is the average enthalpy per particle, which for a single-component system with N particles is given by $\langle h \rangle = \langle H \rangle / N$, where H is the total system enthalpy. This particular definition with the average enthalpy term subtracted is specifically referred to as the reduced heat-flux density [10]. The quantity in Eq. 5 can be obtained from the above expression by localizing the heat flux at the site of each atom, hence,

$$J_\mu(\vec{x}, t) = \Omega \sum_i J_{i,\mu}(t) \delta^{(3)}(\vec{x} - \vec{r}_i) \quad (25)$$

These definitions are consistent with those derived in Ref. [10]. The the Fourier components are given by,

$$\tilde{J}_\mu(\vec{k}, t) = \frac{1}{\Omega} \int_\Omega J_\mu(\vec{x}, t) e^{-i\vec{k} \cdot \vec{x}} d^3x = \sum_i J_{i,\mu}(t) e^{-i\vec{k} \cdot \vec{r}_i} \quad (26)$$

For $\vec{k} = 0$, this reduces to the standard expression of the heat-flux density used in Green-Kubo calculations of the thermal conductivity[3].

Two different simulation supercells were used to compute response functions. The small supercell contained $N = 4608$ atoms and was orthorhombic with dimensions $3.24\text{nm} \times 3.24 \text{ nm} \times 17.3\text{nm}$. The large supercell was also orthorhombic with $N = 9216$ atoms and dimensions $3.24\text{nm} \times 3.24 \text{ nm} \times 34.5\text{nm}$. Both supercells correspond to placing the atoms at a nearest neighbor distance $2^{1/6}\sigma$ which corresponds to the minimum of the LJ potential. The larger supercell dimensions were chosen to probe nonlocal transport effects over longer wavelengths while still maintaining manageable computational costs.

The equations of motion were integrated using the velocity Verlet algorithm with MD timestep of $\Delta t = 2.152\text{fs}$. Each run was preceded by at least 2.5×10^4 MD steps using a constant temperature algorithm, followed by a much longer run to sample the constant energy ensemble. For $T = 12K$ and $T = 72K$ using the small supercell, 10 independent simulations were performed with 2.49×10^6 total steps used for averaging. For the large supercell, 10 independent calculations at $T = 12K$ were performed with 2.40×10^6 steps used for averaging. For simulations at $72K$ in the large supercell, very slow timescales for the response function required longer averaging times. In this case, 20 independent simulations were performed with a total of 4.80×10^6 steps for averaging. Error bars for the response functions and Green-Kubo thermal conductivity were determined from analysis of the statistics of the independent runs.

4. Results

This section begins with the standard Green-Kubo thermal conductivity κ in the which corresponds to the limit $k \rightarrow 0$ of the response function. In Fig. 1, we plot $\kappa(\tau)$ as a function of the upper limit of integration τ from,

$$\kappa(\tau) = \frac{\Omega}{k_B T^2} \int_0^\tau \langle \tilde{J}(0, \tau) \tilde{J}(0, 0) \rangle d\tau \quad (27)$$

The results in Fig. 1 are plotted for the the supercell with $N = 4608$ atoms at $T = 12K$. It can be seen from Fig. 1 that $\tau \approx 40\text{ps}$ appears to be an adequate integration time to obtain the value of κ , resulting in $\kappa = 1.778Wm^{-1}K^{-1}$. Longer integration times result in values $\kappa \approx 2Wm^{-1}K^{-1}$ but with significantly larger error bars. For $T = 72K$, the value $\kappa = 0.338Wm^{-1}K^{-1}$ was obtained, again using the integration limit $\tau = 40\text{ps}$. Computed thermal conductivity values for LJ solids and liquids have been reported elsewhere[11, 12, 13, 14]. We note that our results are comparable in magnitude to these previous works, but exhibit some differences primarily due to differences in the volume per atom and hence the pressure. Specifically, in each of the calculations reported here, the lattice parameter was chosen to be $a = 2^{2/3}\sigma$, which corresponds to the nearest-neighbor distance exactly at the minimum of the LJ potential, specifically $2^{1/6}\sigma$. By contrast, previous studies have generally chosen the lattice parameter such that the pressure was zero, $p = 0$. These differences result in somewhat lower values for κ at low temperatures, but actually higher values of κ for high temperatures. It has been verified in earlier studies that κ is extremely sensitive to the choice of lattice parameter [12, 13].

The computed values of κ can be used within the context of the kinetic theory of heat transport to determine values for the mean free path Λ . In particular, we assume that $\Lambda = \frac{3\kappa}{C_V v_s}$. For lengths $L \sim \Lambda$ and below, it should be expected that the Fourier theory breaks down. From the calculated values of the bulk modulus and the mass density, the sound velocity was determined to be $v_s = 1110ms^{-1}$. At the lowest temperature simulated here with $\kappa = 1.778Wm^{-1}K^{-1}$, this expression yields $\Lambda \approx 4.5nm$, which is comparable to the cell dimension $L = 17.3nm$. This suggests that at least some of the simulation results described below for finite \vec{k} should correspond to at least partially-ballistic transport. It has also been previously reported that Λ tends to depend strongly on mode frequency and wavelength[4], suggesting that many modes may in fact have a mean free path Λ larger than the simulation supercell.

We first analyze the response functions obtained for the small system with $N = 4608$ particles. In Fig. 2, the real part of the response from Eq. 20 for $T = 12K$ is shown as a function of time τ for a few different wave vectors \vec{k} . In particular we consider only nonzero components along the long direction of the supercell from $k_z = \frac{2\pi}{L}$ to the largest value $k_z = \frac{8\pi}{L}$. Some important features emerge. First, as established from the expression in Eq. 20, the response function zero for $\tau = 0$. This reflects the fact that the response to any input heat pulse is not instantaneous. In fact, the rise time in Fig. 2 to reach the maximum in the response function is characteristic of the period of a longitudinal acoustic (LA) vibration. Assuming linear dispersion, which should be approximately true in the long-wavelength limit, this implies for the longest wavelength $\lambda = L = 17.3nm$ a vibrational period $\tau \approx 15.6\text{ps}$. In fact, the maximum response for $k = \frac{2\pi}{L}$ in Fig. 3 occurs

at about $\tau = 6.9\text{ps}$ which is close to half of this vibrational period. Moreover, the response is quite small beyond $\sim 16\text{ps}$, indicating that any perturbation is quickly dissipated in the time it requires the relevant vibrational mode to propagate across the simulation cell. For shorter wavelengths, the response is faster and the time required for the response function to become zero is also shorter. In fact, the times required to reach a maximum are all consistent with half a vibrational period for the relevant LA vibrational mode. The facts demonstrate that for $T = 12K$, transport over length scales $L \leq 17.3\text{nm}$, transport is almost completely ballistic and hence not described by Fourier's law.

In contrast to the ballistic behavior seen in Fig. 2 at $T = 12K$, at $T = 72K$ diffusive behavior begins to emerge. The results in Fig. 3 show $\tilde{K}(k, \tau)$ from simulations at $T = 72K$. In each case, the rise time is comparable to the $T = 12K$ results in Fig. 3. However, especially in the case $k_z = \frac{2\pi}{L}$, the fluctuation persists for a very long time. For $k_z = \frac{4\pi}{L}$ the differences between Fig. 2 and Fig. 3 are noticeable but less dramatic. However, for the cases $k_z = \frac{6\pi}{L}$ and $k_z = \frac{8\pi}{L}$ which correspond to very short length scales, the differences between Fig. 2 and Fig. 3 are very small, indicating that even at the high temperature $T = 72K$ transport is essentially ballistic at these scales.

The real part of the response function $Re \left[\tilde{K}_T(\vec{k}, \omega) \right]$ is shown in Fig. 4 for $T = 12K$ and $k_z = \frac{2\pi}{L}$. In Fig. 5, the imaginary part $Im \left[\tilde{K}_T(\vec{k}, \omega) \right]$ is shown. In generating the data, only the real part of $\tilde{K}(\vec{k}, \tau)$ was used. As previously noted, $\tilde{K}(\vec{k}, \tau)$ is a real function, and any computed imaginary components represent numerical error. For comparison, both Fig. 4 and Fig. 5 show the response functions corresponding to Fourier's theory with $\kappa = 1.778Wm^{-1}K^{-1}$ (see Appendix A). Differences between the computed nonlocal response functions and the Fourier theory demonstrate the ballistic nature of the transport. Interestingly, the results show negative values away from the central peak at $\omega = 0$, which appear to be primarily due to the finite rise time of the response function. The same quantities are shown for $T = 72K$ with $k_z = \frac{2\pi}{L}$ in Fig. 6 and Fig. 7. The comparison between the Fourier theory obtained with $\kappa = 0.338Wm^{-1}K^{-1}$ and the nonlocal response functions show only slight differences, indicating that transport at this higher temperature is mostly diffusive in nature.

The results for the larger simulation cell with length $L = 34.5\text{nm}$ and $N = 9216$ particles show that ballistic behavior persists for $T = 12K$, but the response is even more clearly diffusive at $T = 72K$ in the long wavelength case $k_z = \frac{2\pi}{L}$. In Fig. 8, the response function $Re \left[\tilde{K}_T(\vec{k}, \tau) \right]$ is shown for the large simulation cell at $T = 12K$ for only $k_z = \frac{2\pi}{L}$ and $k_z = \frac{4\pi}{L}$. For $k_z = \frac{2\pi}{L}$, the data appears to have a strong ballistic component, but a longer tail beyond $\tau \approx 50\text{ps}$ which appears to be diffusive. Hence, at these scales for the very low temperature $T = 12K$, partially ballistic behavior persists up to $L = 34.5\text{nm}$. Finally, the result for $k_z = \frac{4\pi}{L}$ looks very close to the results for the small system with $k_z = \frac{2\pi}{L}$ shown in Fig. 2. In Fig. 9, the response $Re \left[\tilde{K}_T(\vec{k}, \omega) \right]$ is shown with comparison to Fourier's theory. In comparison to Fig. 4, the results in Fig. 9 appear closer to Fourier's theory, but the differences are still very noticeable. This is consistent with the picture that with increasing length scales, the response should be closer the diffusive behavior assumed by Fourier's law.

At $T = 72\text{K}$ for the large system with length $L = 34.5\text{nm}$, the transport behavior appears increasingly diffusive. In Fig. 10, the response function $\text{Re} \left[\tilde{K}_T(\vec{k}, \tau) \right]$ is shown. For $k_z = \frac{2\pi}{L}$, even after $\tau \approx 400\text{ps}$, it isn't clear that the response function has converged to zero. The requirement for very long integration times makes it difficult to obtain a converged function, which is indicated by the rather large error bars. Because of the large error bars we do not show the Fourier-transformed response functions. However, the results in Fig. 10 demonstrate diffusive behavior very clearly. For example, the time required for convergence to zero should depend on length as $\sim L^2$ for diffusive transport(see Appendix A). The results in Fig. 10 approximately demonstrate this relationship. By contrast, ballistic transport would correspond to a dissipation time which depends on linearly on system length. However, is still likely that the results in Fig. 10 show some partially ballistic behavior.

Given the response function $\tilde{K}_T(\vec{k}, \omega)$, the temperature profile can be computed as a response to any external heat source. The details of the calculations are given in Appendix A both for any general response function $\tilde{K}_T(\vec{k}, \omega)$ and specifically for Fourier's law. Here we specifically consider the response to a very simple sinusoidal heat source given by,

$$\frac{\partial \Delta h^{(ext)}(\vec{x}, t)}{\partial t} = \frac{1}{4} a (e^{i\omega t} + e^{-i\omega t}) \left(e^{i\vec{k}\cdot\vec{x}} + e^{-i\vec{k}\cdot\vec{x}} \right) = a \cos(\vec{k}\cdot\vec{x}) \cos(\omega t) \quad (28)$$

Here we will consider $\vec{k} = \frac{2\pi}{L} \hat{z}$, where L is the system length along the long direction of the MD simulations described above. For this length, as noted previously, partially-ballistic results are seen at low temperatures, whereas the behavior becomes more consistent with Fourier's law at higher temperatures. The temperature profiles are given by Eq. 31 in Appendix A when $\tilde{K}_T(\vec{k}, \omega)$ is obtained from the MD simulations for the small system. For the behavior given by Fourier's law, the temperature profile is described by Eq. 35 also in Appendix A.

The results of this comparison are shown in Figs. 11-13 for an external source with frequency $\frac{\omega}{2\pi} = 0.012\text{THz}$ at the average temperature $T = 12\text{K}$. It is assumed in these calculations that the source has been active for a very long period of time so that any transient phenomena can be neglected. For the heating rate we chose a value $a\Omega = 18.1\text{nW}$ which results in small enough temperature deviations to assume that the linear-response theory applies. Note that because of the form of the external source in Eq. 28, the external source does not change the overall average system temperature.

In Fig. 11 and Fig. 12, temperature profiles $T(z, t)$ are shown for the nonlocal theory and Fourier's law assuming $\kappa = 1.778\text{Wm}^{-1}\text{K}^{-1}$ corresponding to the average temperature $T = 12\text{K}$. At time $t = 0$, the external source is adding heat near $z = 0$ and $z = L$, and removing heat at $z = \frac{L}{2}$ at a maximum rate. At $t = 0$, the differences between the two theories is rather small as shown in Fig. 11. By contrast, at the intermediate time, $t = \frac{\pi}{2\omega}$, when the amplitude of the external source is instantaneously zero, there is a dramatic difference between the two theories, with smaller dissipation in the nonlocal theory. The reason for the difference is due both to a different phase angle δ and also a different magnitude of the response function $\tilde{K}_T(\vec{k}, \omega)$ predicted by the two theories. At $T = 72\text{K}$, the nonlocal theory is expected to predict similar response in comparison to Fourier's theory. In Fig. 13, a comparison is made at time $t = \frac{\pi}{2\omega}$ where

the difference should be most significant. However, the differences are actually quite small as suggested by the similarity in the response function $\tilde{K}_T(\vec{k}, \omega)$ at $T = 72\text{K}$ shown in Fig. 6 and Fig. 7.

The response function $\tilde{K}_T(\vec{k}, \omega)$ can also be used to determine the effective thermal conductivity κ_{eff} in the static limit of the external source $\omega \rightarrow 0$. This limit corresponds, for example, to the effective thermal conductivity which is derived from applying the Fourier law to the steady-state temperature profile that is measured or computed in response to a static heat source and sink. In an MD simulation, this corresponds to the usual “direct” method of determining κ_{eff} [3]. It is known that the effective thermal conductivity κ_{eff} determined in MD simulations using the “direct” method, as was previously discussed, strongly dependent on system size L when $L \sim \Lambda$, where Λ is the mean-free path for heat carriers. In the results reported here, this will be seen as a dependence of κ_{eff} on wave vector k . The details of the theory are left to Appendix A, where we derive the final result in Eq. 37 for the dependence $\kappa_{eff}(k)$. Note also that given enough data for very large simulation cells, taking the limit $k \rightarrow 0$ should correspond to the bulk thermal conductivity κ shown in Fig. 2.

To determine $\kappa_{eff}(k)$, we will consider the smallest frequency $\frac{\omega}{2\pi} = 0.012\text{THz}$ to approximate the limit $\omega \rightarrow 0$. For $T = 12\text{K}$ and $T = 72\text{K}$, the results are shown in Fig. 14 as a plot of $\frac{1}{\kappa_{eff}}$ as a function of inverse length scale $\frac{k}{2\pi}$. Also included in Fig. 14 are the results obtained for the large system with $L = 34.5\text{nm}$ at $k_z = \frac{2\pi}{L}$. In addition, the Green-Kubo results from Eq.3 are included for $\frac{k}{2\pi} = 0$. The results in Fig. 14 are quite similar to the dependence of the effective thermal conductivity on inverse system size seen in Ref. [3] and elsewhere. Qualitatively, the results demonstrate that partially-ballistic transport over short length scales results in smaller effective conductivity values in comparison to the bulk conductivity.

5. Discussion and conclusions

The results in this article demonstrate how nonlocal transport properties can be determined using the Green-Kubo approach. Response functions were computed to describe the effective of an external heat source acting on a LJ solid, with comparisons made to Fourier’s law to elucidate nonlocal heat transport phenomena, including transport in the partially-ballistic regime. In Appendix A, the expression for $K_T(\vec{k}, \omega)$ is obtained for an isotropic medium (e.g. for a cubic crystal) using Fourier’s law. In Fourier’s law, the only relevant quantities are the thermal conductivity κ and the volumetric specific heat capacity c_V which can be combined to obtain the thermal diffusivity $\alpha = \frac{\kappa}{c_V}$.

It was shown how quantitative determination of the response functions $K_T(\vec{k}, \omega)$ can be used to simulate the response of a system to an external heat source without the need to perform additional MD simulations. Details of this approach are given in Appendix A along with corresponding expressions obtained from Fourier’s law. It was shown that at low temperatures and relatively short length scales that transport becomes partially ballistic and Fourier’s law predicts substantially different results.

Finally, it was demonstrated how to obtain values for the effective thermal conductivity $\kappa_{eff}(k)$ corresponding to the response of a system to a static external heat source. As with the effective conductivity

obtained using the “direct” method, partially-ballistic transport for finite length scales results in effective conductivity values lower than those obtained in the limit $k \rightarrow 0$. Therefore, we have demonstrated how Green-Kubo results for the response functions $K_T(\vec{k}, \omega)$ in the limit $\omega \rightarrow 0$ can be used to interpret or predict the results of “direct” MD simulations of thermal transport.

We suggest that simulation results for $K_T(\vec{k}, \omega)$ be used to model the response of systems to external heat sources, especially in regimes where partially ballistic transport is relevant. Specifically, when transport is measured over distances smaller than the mean free path Λ and heat waves with transport is primarily limited by the sound velocity can be analyzed and modeled using the approach outlined here. It would also be useful and interesting to compare the response functions obtained from the Green-Kubo methods to predictions from other approaches which go beyond Fourier’s law, including the Cattaneo-Vernotte equations [15, 16], enhanced Fourier’s law[17], dual-phase lag model[18], and the mean-free path accumulation function[19]. It would also be interesting to use this approach to elucidate transport in superlattices, where it has been difficult to connect transport properties to the phonon spectrum of the superlattice in the limit where the mean free path is expected to be larger than the superlattice spacing.

6. Acknowledgments

We acknowledge use of the STOKES cluster provided by the ARCC at UCF. We also would like to acknowledge support from the UCF Burnett Honor’s College, and also very useful discussions and inspiration from Prof. Philip Allen.

7. Appendix A

Here we derive the time-dependent temperature profiles shown in the previous section and also obtain the expression for the effective thermal conductivity $\kappa_{eff}(\vec{k})$. Using the response function $\tilde{K}_T(\vec{k}, \omega)$, it is very straightforward to show that the heat-flux density which results from the external perturbation in Eq. 28 is given by,

$$\vec{J}(\vec{x}, t) = \vec{k} \left(\frac{a\Omega}{C_p} \right) |\tilde{K}_T(\vec{k}, \omega)| \cos(\omega t - \delta) \sin(\vec{k} \cdot \vec{x}) \quad (29)$$

in which $|\tilde{K}_T(\vec{k}, \omega)| = \left[\tilde{K}_T(\vec{k}, -\omega) \tilde{K}_T(\vec{k}, \omega) \right]^{\frac{1}{2}}$. The phase angle δ is given by,

$$\tan \delta = -\frac{Im \left[\tilde{K}_T(\vec{k}, \omega) \right]}{Re \left[\tilde{K}_T(\vec{k}, \omega) \right]} \quad (30)$$

Including the external source term, the temperature profile is given by,

$$T(\vec{x}, t) = T_0 - \left(\frac{a\Omega}{C_p\omega} \right) \left[\left(\frac{\Omega}{C_p} \right) k^2 |\tilde{K}_T(\vec{k}, \omega)| \sin(\omega t - \delta) - \sin(\omega t) \right] \cos(\vec{k} \cdot \vec{x}) \quad (31)$$

in which T_0 is the average temperature of the system. Using numerical results for the response function $\tilde{K}_T(\vec{k}, \omega)$, the temperature profile can easily be computed as a function of time. Note that there is an

implicit assumption that the external perturbation has been active for a very long period of time such that any transient behavior can be ignored.

The response function can be determined using Fourier's law for comparison. In this case, it is easy to demonstrate that the response function is given by,

$$\tilde{K}_T(\vec{k}, \omega) = \kappa \int_0^\infty e^{-\alpha k^2 \tau} e^{-i\omega \tau} d\tau = \kappa \left[\frac{\alpha k^2 - i\omega}{(\alpha k^2)^2 + \omega^2} \right] \quad (32)$$

in which α is the thermal diffusivity. Given the response function determined using Fourier's law, the external perturbation in Eq. 28 results in the heat-flux density,

$$\vec{J}(\vec{x}, t) = \vec{k} \left(\frac{a\Omega\kappa}{C_p} \right) \frac{\cos(\omega t - \delta)}{[(\alpha k^2)^2 + \omega^2]^{\frac{1}{2}}} \sin(\vec{k} \cdot \vec{x}) \quad (33)$$

with the relative phase angle given by,

$$\tan \delta = \frac{\omega}{\alpha k^2} \quad (34)$$

Finally, the temperature profile is given by,

$$T(\vec{x}, t) = T_0 - \left(\frac{a\Omega}{C_p \omega} \right) \left[\left(\frac{\kappa\Omega}{C_p} \right) \frac{k^2 \sin(\omega t - \delta)}{[(\alpha k^2)^2 + \omega^2]^{\frac{1}{2}}} - \sin(\omega t) \right] \cos(\vec{k} \cdot \vec{x}) \quad (35)$$

In the case of Fourier's law, it can be verified from the expressions for $\vec{J}(\vec{x}, t)$ and $T(\vec{x}, t)$ that the thermal conductivity κ is recovered from,

$$\kappa = - \lim_{\omega \rightarrow 0} \frac{\vec{k} \cdot \vec{J}}{\vec{k} \cdot \vec{\nabla} T} \quad (36)$$

In the more general case with nonlocal response, the effective thermal conductivity $\kappa_{eff}(\vec{k})$ is then defined in the same way, with the resulting expression,

$$\kappa_{eff}(\vec{k}) = - \frac{C_p}{\Omega k^2} \lim_{\omega \rightarrow 0} \frac{Re \left[\omega \tilde{K}_T(\vec{k}, \omega) \right]}{Im \left[\tilde{K}_T(\vec{k}, \omega) \right]} \quad (37)$$

Then one recovers the thermal conductivity from taking the limit of this expression to $\vec{k} = 0$, namely $\kappa = \lim_{\vec{k} \rightarrow 0} \kappa_{eff}(\vec{k})$. For the results shown in Fig. 14, we have used $C_p \approx C_V = 3Nk_B$ where C_V is the constant-volume heat capacity evaluated in the harmonic limit, which is appropriate for the crystalline system considered in this paper.

References

- [1] D. G. Cahill, W. K. Ford, K. E. Goodson, G. D. Mahan, A. Majumdar, H. J. Maris, R. Merlin, and S. R. Phillpot, “Nanoscale thermal transport,” *J. Appl. Phys.* **93**, 793 (2003)
- [2] D. G. Cahill, P. V. Braun, G. Chen, D. R. Clarke, S. Fan, K. E. Goodson, P. Keblinski, W. P. King, G. D. Mahan, A. Majumdar, H. J. Maris, S. R. Phillpot, E. Pop, and L. Shi, “Nanoscale thermal transport II. 2003-2012,” *Appl. Phys. Rev.* **1**, 011305 (2014)
- [3] P. K. Schelling, S. R. Phillpot, and P. Keblinski, “Comparison of atomic-level simulation methods for computing thermal conductivity,” *Phys. Rev. B* **65**, 144306 (2002)
- [4] D. P. Sellan, E. S. Landry, J. E. Turney, A. J. H. McGaughey, and C. H. Amon, “Size effects in molecules dynamics thermal conductivity predictions,” *Phys. Rev. B* **81** (21), 214305 (2010)
- [5] P. B. Allen, “Analysis of nonlocal phonon thermal conductivity simulations showing ballistic to diffusive crossover,” *Phys. Rev. B* **97**, 134307 (2018)
- [6] X. W. Zhou, S. Aubry, R. E. Jones, A. Greenstein, and P. K. Schelling “Towards more accurate molecules dynamics calculations of thermal conductivity: Case study of GaN bulk crystals,” *Phys. Rev. B* **79**, 115201 (2009)
- [7] R. Kubo, “Statistical-mechanical theory of irreversible processes. I. General Theory and Simple Applications to Magnetic and Conduction Problems,” *J. Phys. Soc. Japan* **12** (6), 570 (1957)
- [8] M. S. Green, “Markoff Random Processes and the Statistical Mechanics of TimeDependent Phenomena. II. Irreversible Processes in Fluids,” *J. Chem. Phys.* **22** (3), 398 (1954)
- [9] G. D. Mahan and F. Claro, “Nonlocal theory of thermal conductivity,” *Phys. Rev. B* **38**, 1963 (1988)
- [10] J. H. Irving and J. G. Kirkwood, “The Statistical Mechanical Theory of Transport Processes. IV. The Equations of Hydrodynamics,” *J. Chem. Phys.* **18**, 817 (1950)
- [11] K. V. Tretiakov and S. Scandolo, “Thermal conductivity of solid argon from molecular dynamics simulation,” *J. Chem. Phys.* **120** 3765 (2004)
- [12] A. J. H. McGaughey and M. Kaviani, “Quantitative validation of the Boltzmann transport equation phonon thermal conductivity model under the single-mode relation time approximation,” *Phys. Rev. B* **69**, 094303 (2004)
- [13] H. Kaburaki, J. Li, S. Yip, H. Kimizuka, “Dynamical thermal conductivity of argon crystal,” *J. Appl. Phys.* **102**, 043514 (2007)
- [14] H. Revollo and S. Curilef, “Thermal conductivity of argon: Modeling and comparison with experimental data,” *J. Phys. Conf. Ser.* **1043**, 012010 (2018)

- [15] C. Cattaneo, “A form of heat conduction which eliminates the paradox of instantaneous propagation,” *Compte Rendus* **247**, 431 (1958)
- [16] P. Vernotte, “Some possible complications in the phenomena of thermal conduction,” *Compte Rendus* **252**, 2190 (1961)
- [17] A. T. Ramu, “An enhanced Fourier law derivable from the Boltzmann transport equation and a sample application in determining the mean-free path of nondiffusive phonon modes”, *J. Appl. Phys.* **116**, 093501 (2014)
- [18] D. Y. Tzou, “The generalized lagging response in small-scale and high-rate heating,” *Int. J. Heat Mass Trans., ASME Trans.* **117**, 8 (1995)
- [19] C. Dames, and G. Chen, “Thermal conductivity of nanostructured thermoelectric materials,” *Thermoelectrics Handbook: Macro to Nano*, Chapter 42, CRC Press, ed. D. Rowe, (2005)

Figure Captions

Figure 1 Green-Kubo integral from Eq. 27 as a function of the upper limit of integration τ for $T = 12K$. The error bars were determined from statistical analysis of several independent simulations. This result is for the system with $N = 4608$ atoms.

Figure 2 Real part of the integral in Eq. 20 for $\tilde{K}(\vec{k}, \tau)$ at temperature $T = 12K$ as a function of integration limit τ for various values of $\vec{k} = k_z \hat{z}$. Error bars not shown in instances where they are smaller than the symbols.

Figure 3 Real part of the integral in Eq. 20 for $\tilde{K}(\vec{k}, \tau)$ at temperature $T = 72K$ as a function of integration limit τ for various values of $\vec{k} = k_z \hat{z}$. Error bars not shown in instances where they are smaller than the symbols.

Figure 4 Real part of the Fourier transform $\tilde{K}_T(\vec{k}, \omega)$ from Eq. 21 at $T = 12K$ as a function of frequency $\frac{\omega}{2\pi}$ for $k_z = \frac{2\pi}{L}$. Comparison is made to the response function given by Fourier's law.

Figure 5 Imaginary part of the Fourier transform $\tilde{K}_T(\vec{k}, \omega)$ from Eq. 21 at $T = 12K$ as a function of frequency $\frac{\omega}{2\pi}$ for $k_z = \frac{2\pi}{L}$. Comparison is made to the response function given by Fourier's law.

Figure 6 Real part of the Fourier transform $\tilde{K}_T(\vec{k}, \omega)$ from Eq. 21 at $T = 72K$ as a function of frequency $\frac{\omega}{2\pi}$ for $k_z = \frac{2\pi}{L}$. Comparison is made to the response function given by Fourier's law.

Figure 7 Imaginary part of the Fourier transform $\tilde{K}_T(\vec{k}, \omega)$ from Eq. 21 at $T = 72K$ as a function of frequency $\frac{\omega}{2\pi}$ for $k_z = \frac{2\pi}{L}$. Comparison is made to the response function given by Fourier's law.

Figure 8 Real part of the integral in Eq. 20 for $\tilde{K}(\vec{k}, \tau)$ at temperature $T = 12K$ as a function of integration limit τ for $k_z = \frac{2\pi}{L}$ and $k_z = \frac{4\pi}{L}$. These results were obtained for the large system size with $L = 34.5\text{nm}$ and $N = 9216$ particles.

Figure 9 Real part of $\tilde{K}_T(\vec{k}, \omega)$ from the nonlocal theory compared with the same quantity from Fourier's law for $T = 12K$ with $k_z = \frac{2\pi}{L}$. These results were obtained for the larger system size with $L = 34.5\text{nm}$ and $N = 9216$ particles.

Figure 10 Real part of the integral in Eq. 20 for $\tilde{K}(\vec{k}, \tau)$ at temperature $T = 72K$ as a function of integration limit τ for $k_z = \frac{2\pi}{L}$ and $k_z = \frac{4\pi}{L}$. These results were obtained for the larger system size with $L = 34.5\text{nm}$ and $N = 9216$ particles.

Figure 11 Temperature profiles obtained from the nonlocal response function (solid red line) and Fourier's law (dashed green line) for an input heat source given by Eq. 28. Results shown for time $t = 0$ with average temperature $T = 12K$.

Figure 12 Temperature profiles obtained from the nonlocal response function (solid red line) and Fourier's law (dashed green line) for an input heat source given by Eq. 28. Results shown for time $t = \frac{\pi}{2\omega}$ with average temperature $T = 12K$.

Figure 13 Temperature profiles obtained from the nonlocal response function (solid red line) and Fourier's law (dashed green line) for an input heat source given by Eq. 28. Results shown for time $t = \frac{\pi}{2\omega}$ with average temperature $T = 72K$.

Figure 14 Inverse effective conductivity κ_{eff}^{-1} as a function of inverse length $\frac{k}{2\pi}$ in units σ^{-1} obtained from the nonlocal simulation results and Eq. 37. Values for $k = 0$ obtained from the standard Green-Kubo equation for κ .

Figure 1: Green-Kubo integral from Eq. 27 as a function of the upper limit of integration τ for $T = 12K$. The error bars were determined from statistical analysis of several independent simulations. This result is for the system with $N = 4608$ atoms.

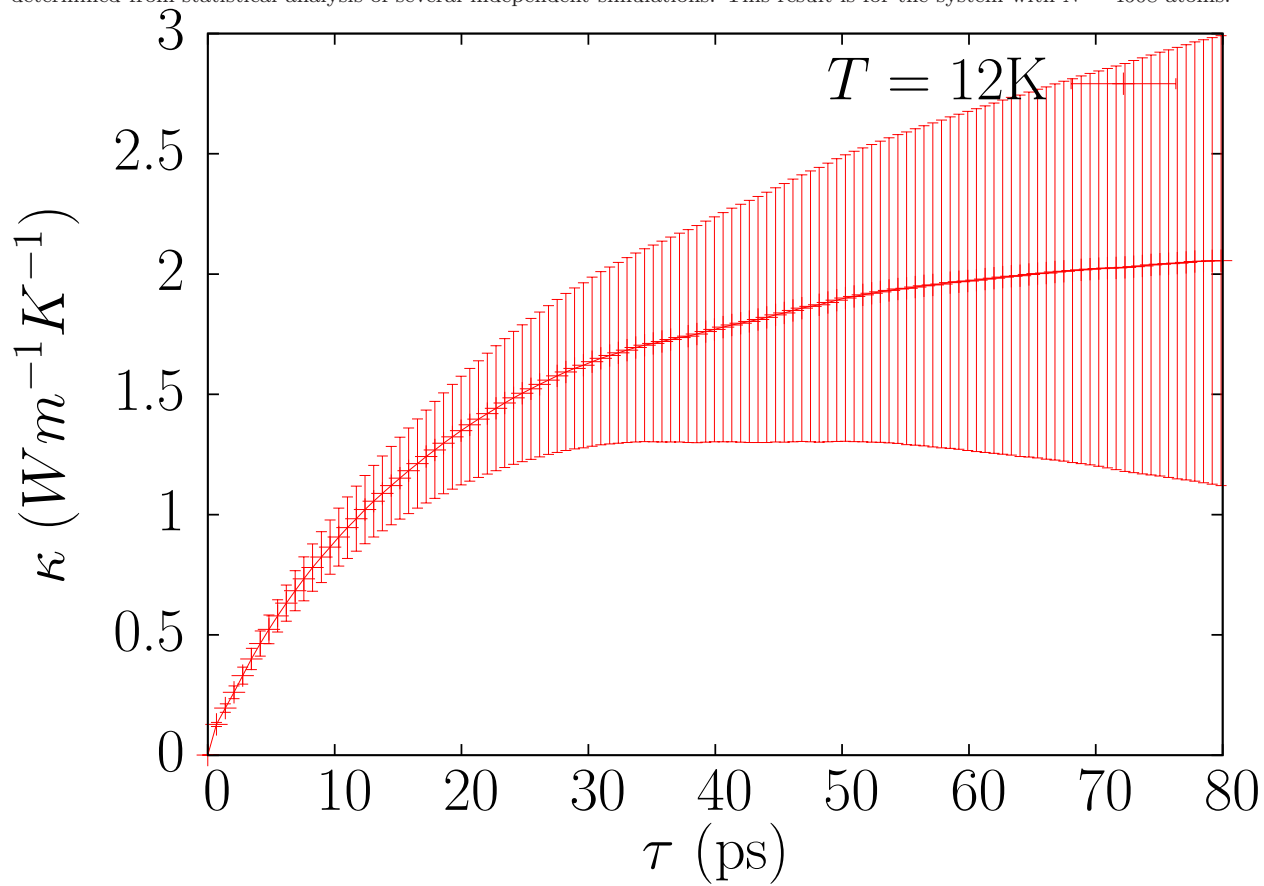


Figure 2: Real part of the integral in Eq. 20 for $\tilde{K}(\vec{k}, \tau)$ at temperature $T = 12K$ as a function of integration limit τ for various values of $\vec{k} = k_z \hat{z}$. Error bars not shown in instances where they are smaller than the symbols.

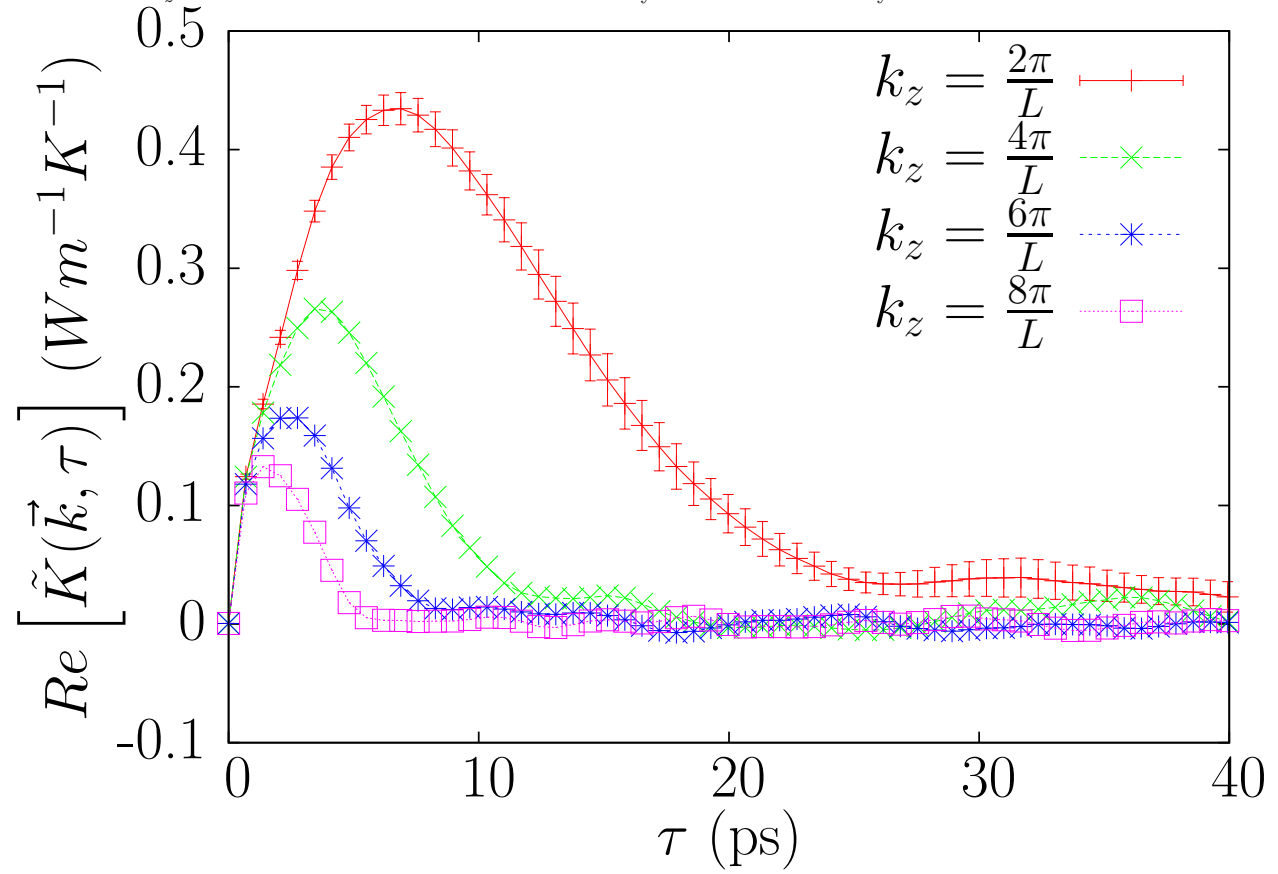


Figure 3: Real part of the integral in Eq. 20 for $\tilde{K}(\vec{k}, \tau)$ at temperature $T = 72K$ as a function of integration limit τ for various values of $\vec{k} = k_z \hat{z}$. Error bars not shown in instances where they are smaller than the symbols.

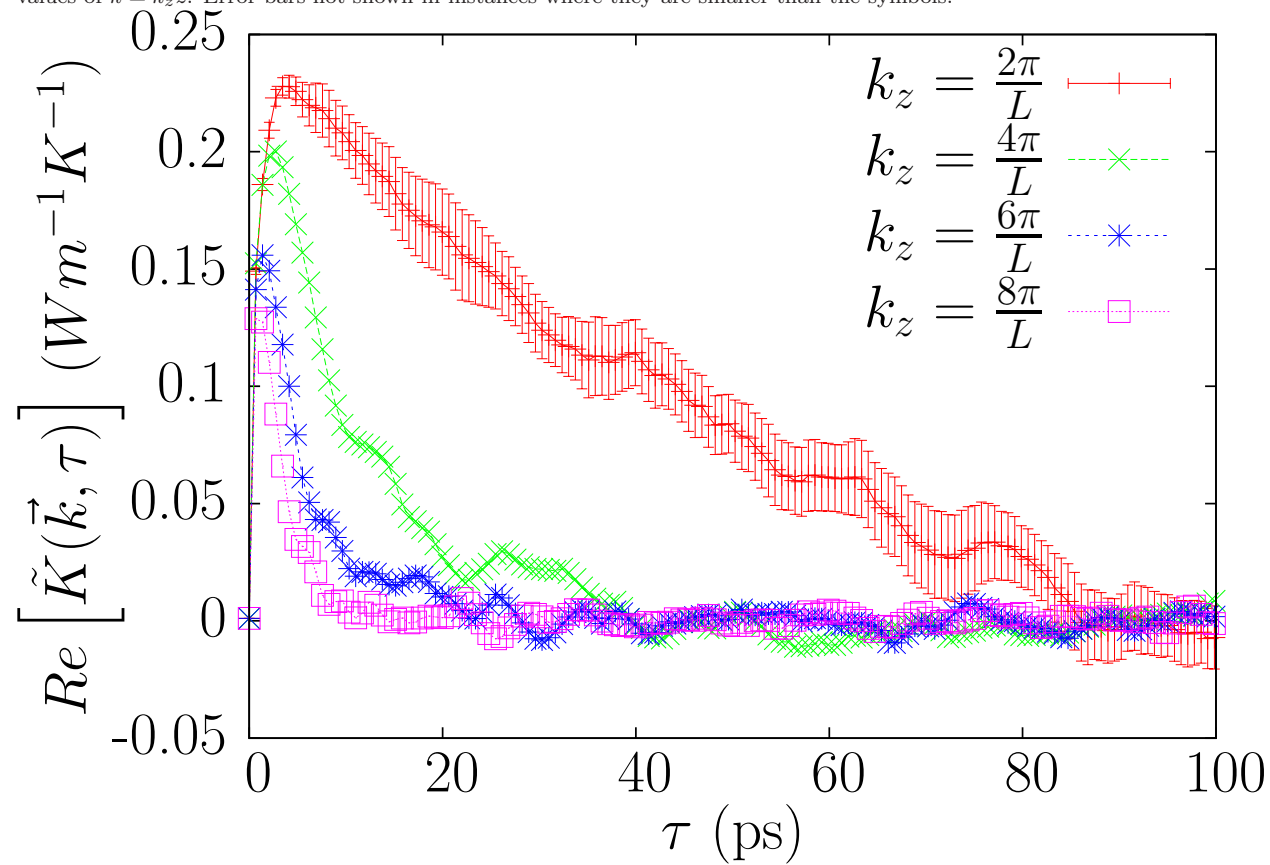


Figure 4: Real part of the Fourier transform $\tilde{K}_T(\vec{k}, \omega)$ from Eq. 21 at $T = 12K$ as a function of frequency $\frac{\omega}{2\pi}$ for $k_z = \frac{2\pi}{L}$. Comparison is made to the response function given by Fourier's law.

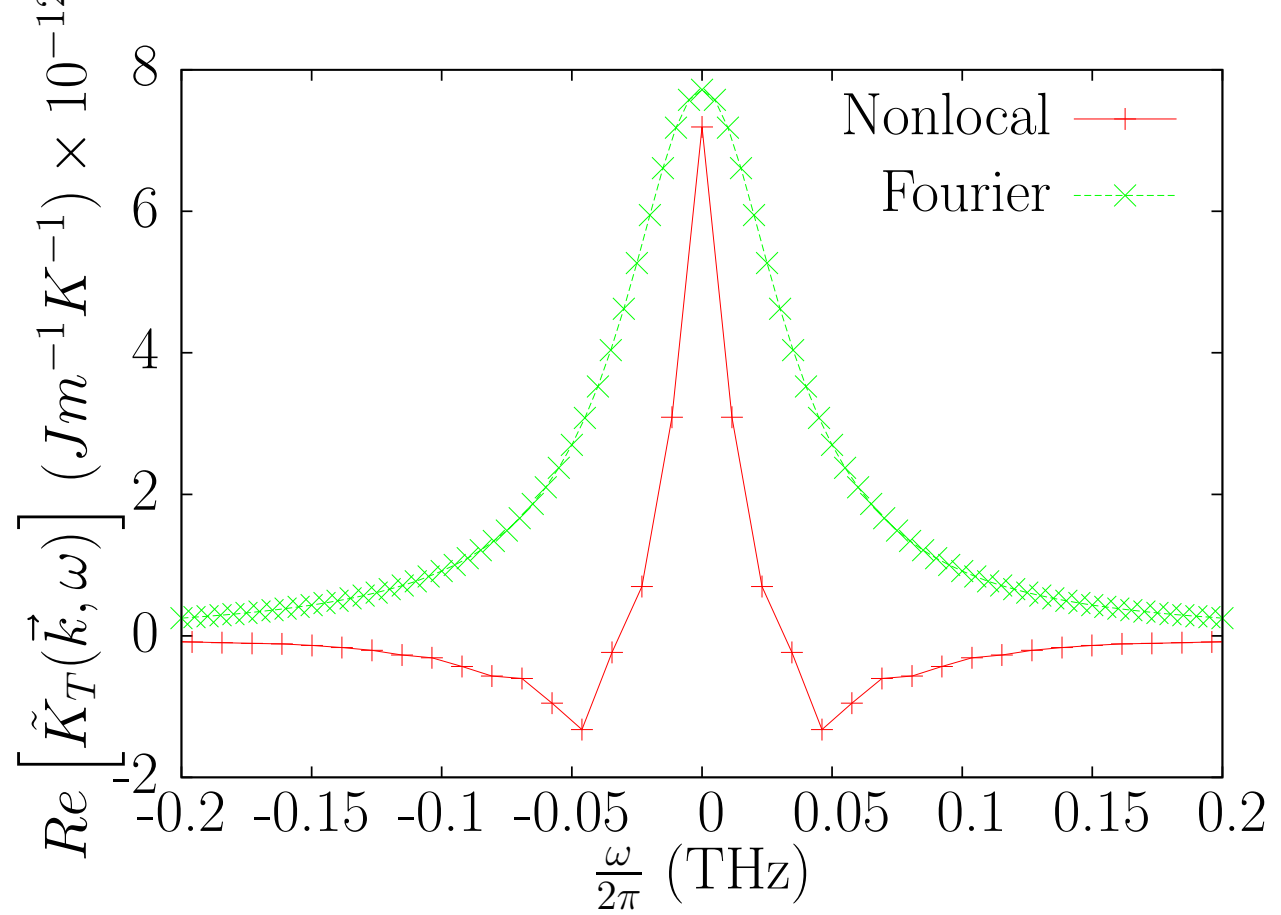


Figure 5: Imaginary part of the Fourier transform $\tilde{K}_T(\vec{k}, \omega)$ from Eq. 21 at $T = 12K$ as a function of frequency $\frac{\omega}{2\pi}$ for $k_z = \frac{2\pi}{L}$. Comparison is made to the response function given by Fourier's law.

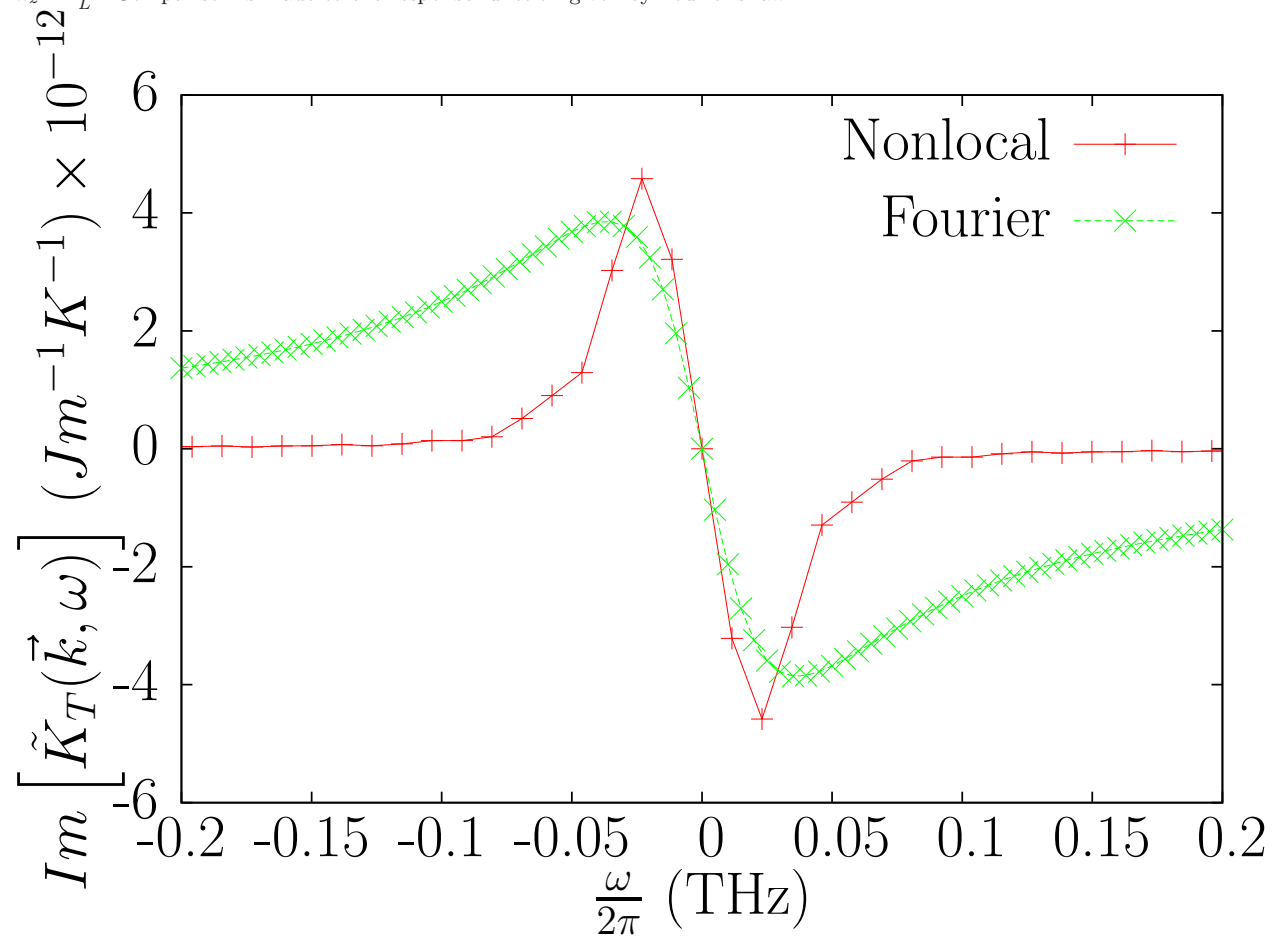


Figure 6: Real part of the Fourier transform $\tilde{K}_T(\vec{k}, \omega)$ from Eq. 21 at $T = 72K$ as a function of frequency $\frac{\omega}{2\pi}$ for $k_z = \frac{2\pi}{L}$. Comparison is made to the response function given by Fourier's law.

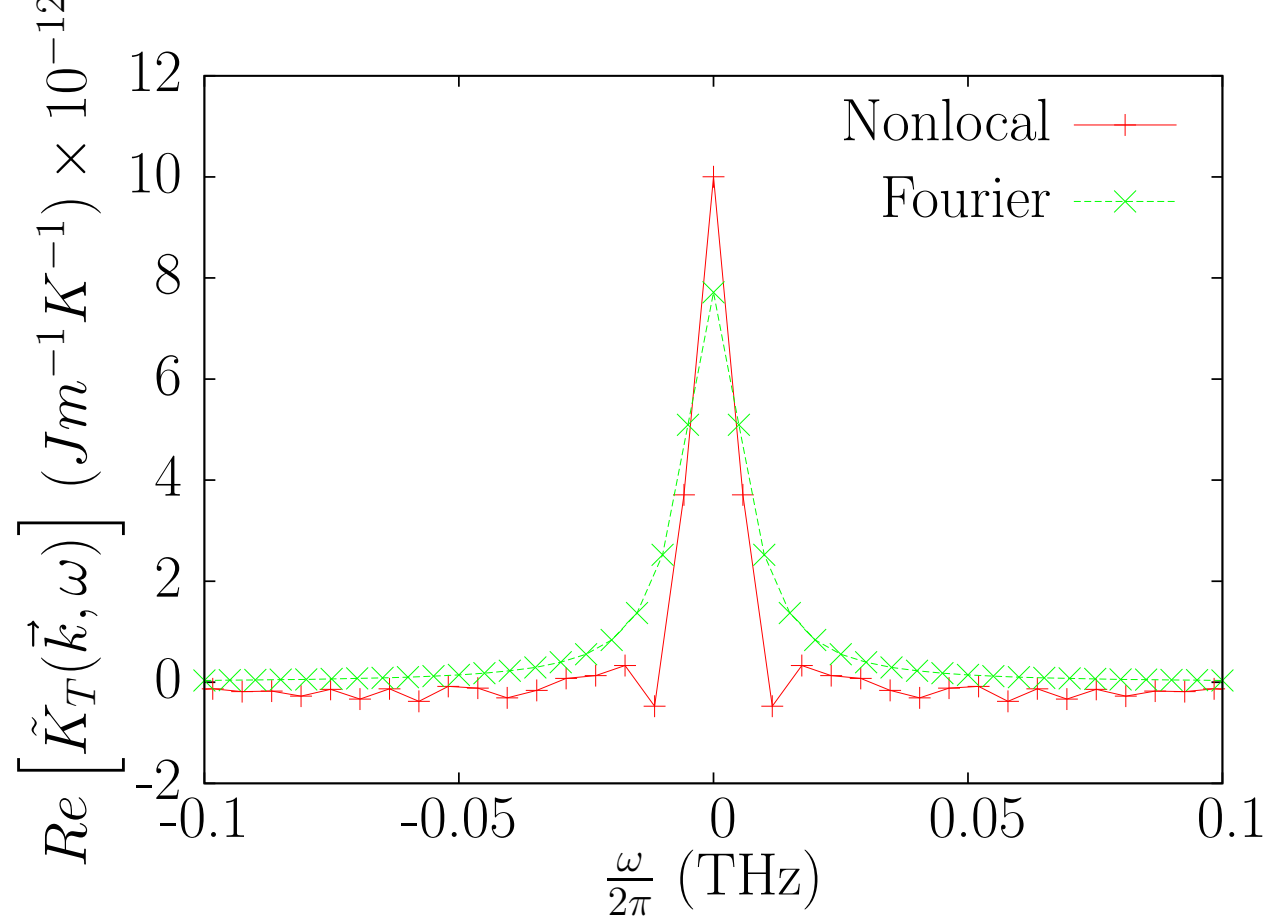


Figure 7: Imaginary part of the Fourier transform $\tilde{K}_T(\vec{k}, \omega)$ from Eq. 21 at $T = 72K$ as a function of frequency $\frac{\omega}{2\pi}$ for $k_z = \frac{2\pi}{L}$. Comparison is made to the response function given by Fourier's law.

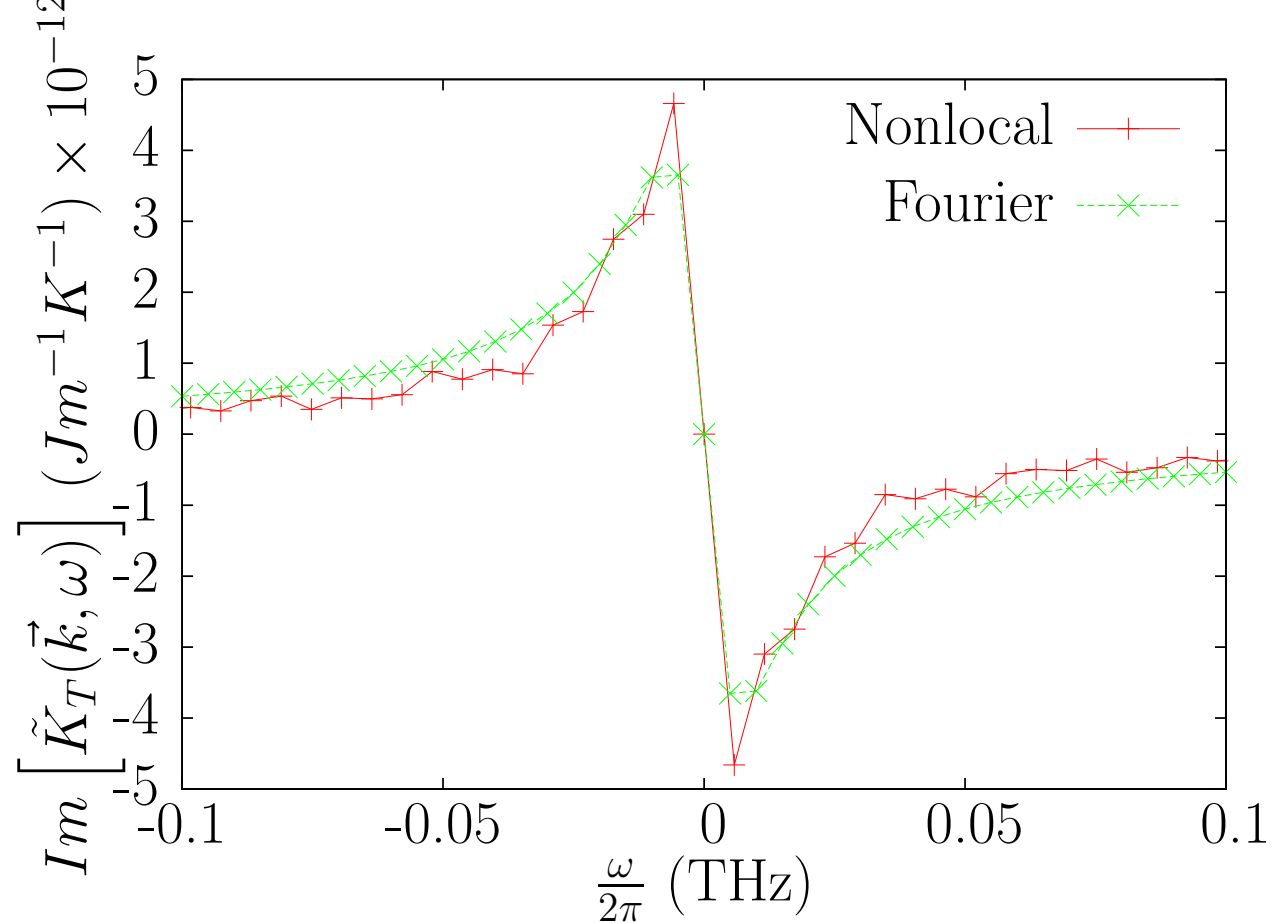


Figure 8: Real part of the integral in Eq. 20 for $\tilde{K}(\vec{k}, \tau)$ at temperature $T = 12K$ as a function of integration limit τ for $k_z = \frac{2\pi}{L}$ and $k_z = \frac{4\pi}{L}$. These results were obtained for the large system size with $L = 34.5\text{nm}$ and $N = 9216$ particles.

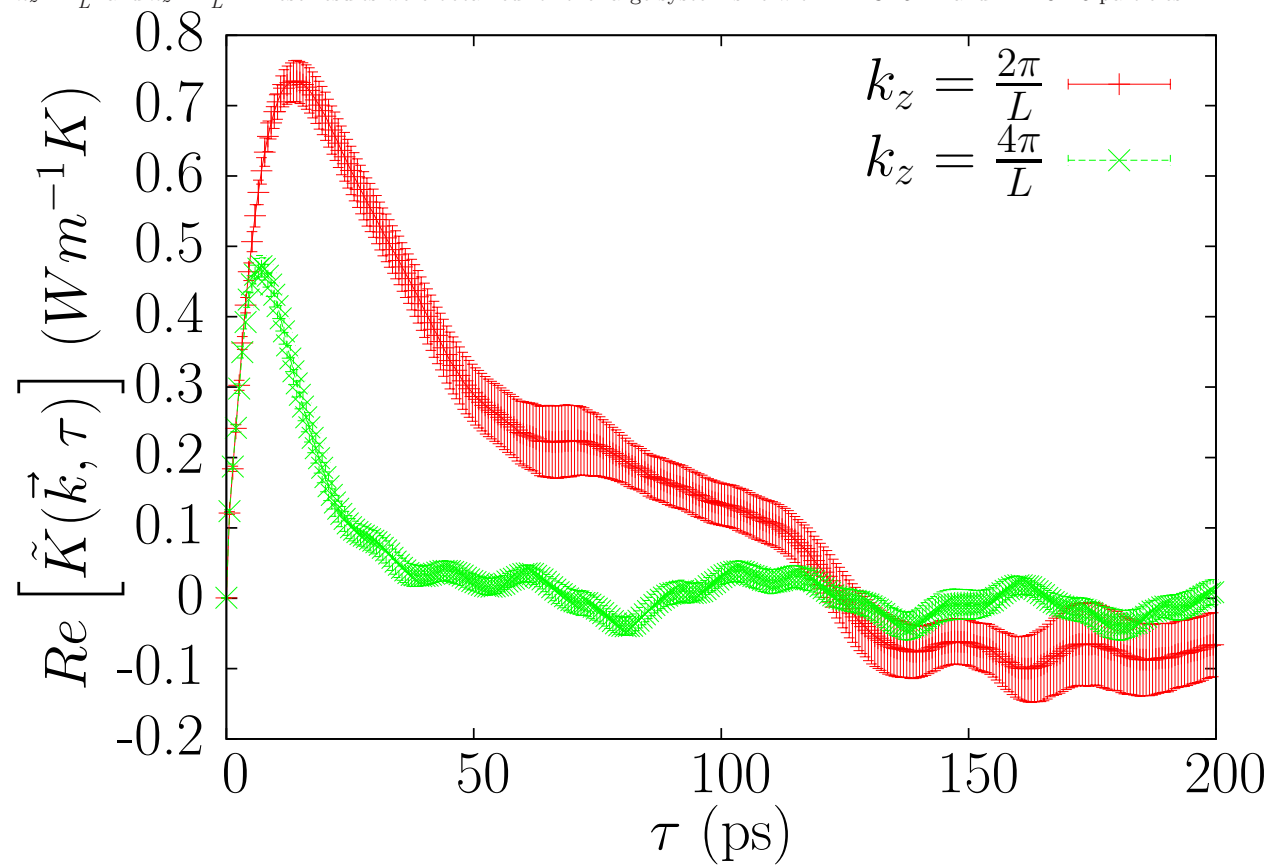


Figure 9: Real part of $\tilde{K}_T(\vec{k}, \omega)$ from the nonlocal theory compared with the same quantity from Fourier's law for $T = 12K$ with $k_z = \frac{2\pi}{L}$. These results were obtained for the larger system size with $L = 34.5\text{nm}$ and $N = 9216$ particles.

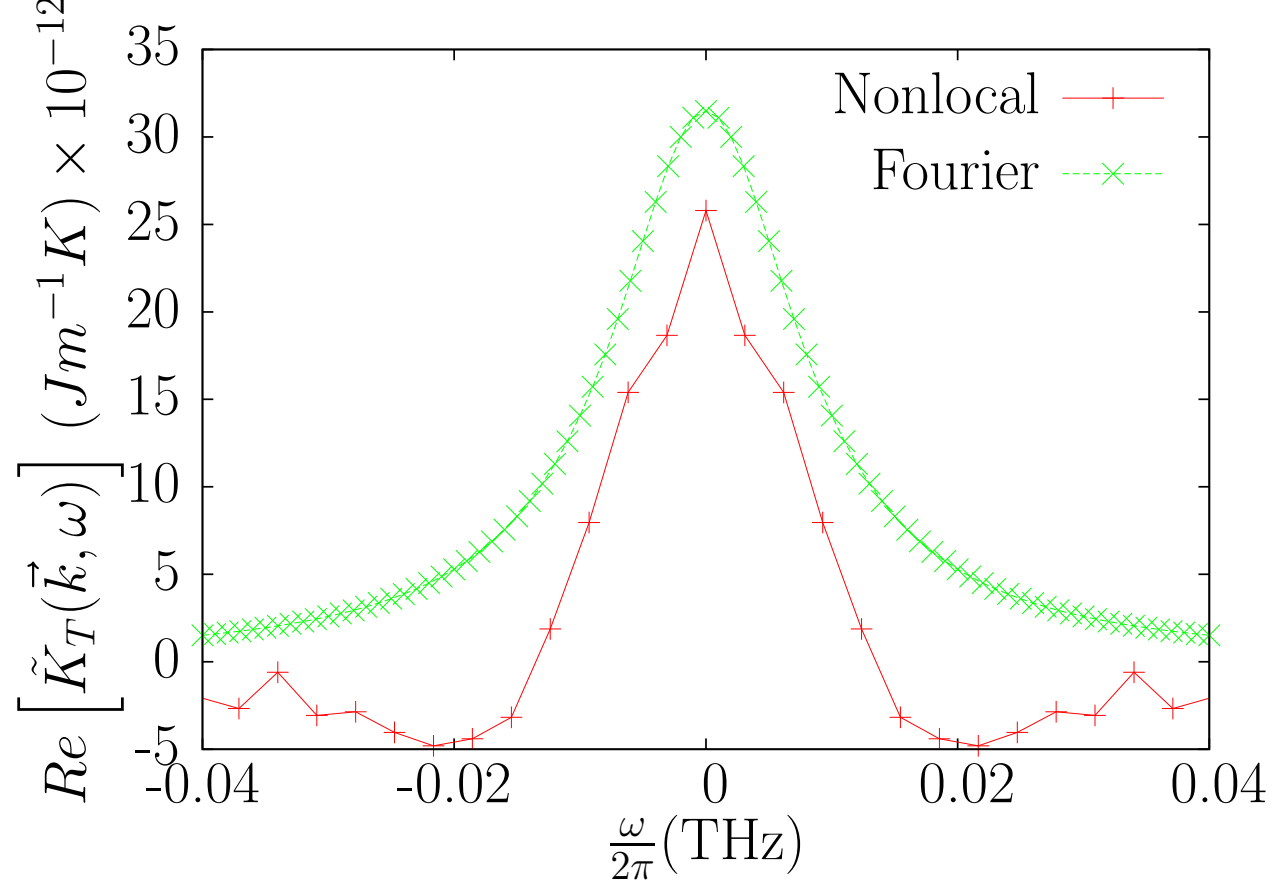


Figure 10: Real part of the integral in Eq. 20 for $\tilde{K}(\vec{k}, \tau)$ at temperature $T = 72K$ as a function of integration limit τ for $k_z = \frac{2\pi}{L}$ and $k_z = \frac{4\pi}{L}$. These results were obtained for the larger system size with $L = 34.5\text{nm}$ and $N = 9216$ particles.

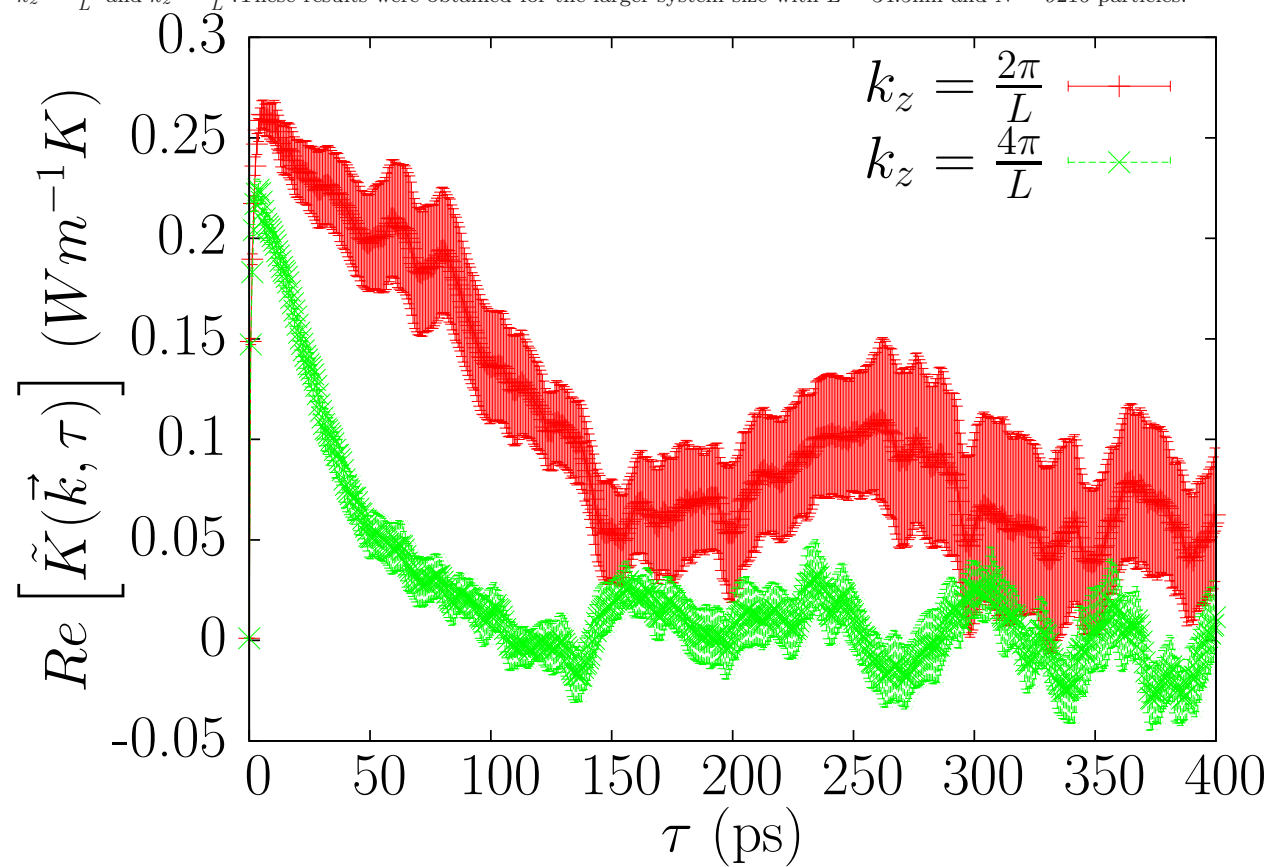


Figure 11: Temperature profiles obtained from the nonlocal response function (solid red line) and Fourier's law (dashed green line) for an input heat source given by Eq. 28. Results shown for time $t = 0$ with average temperature $T = 12\text{K}$.

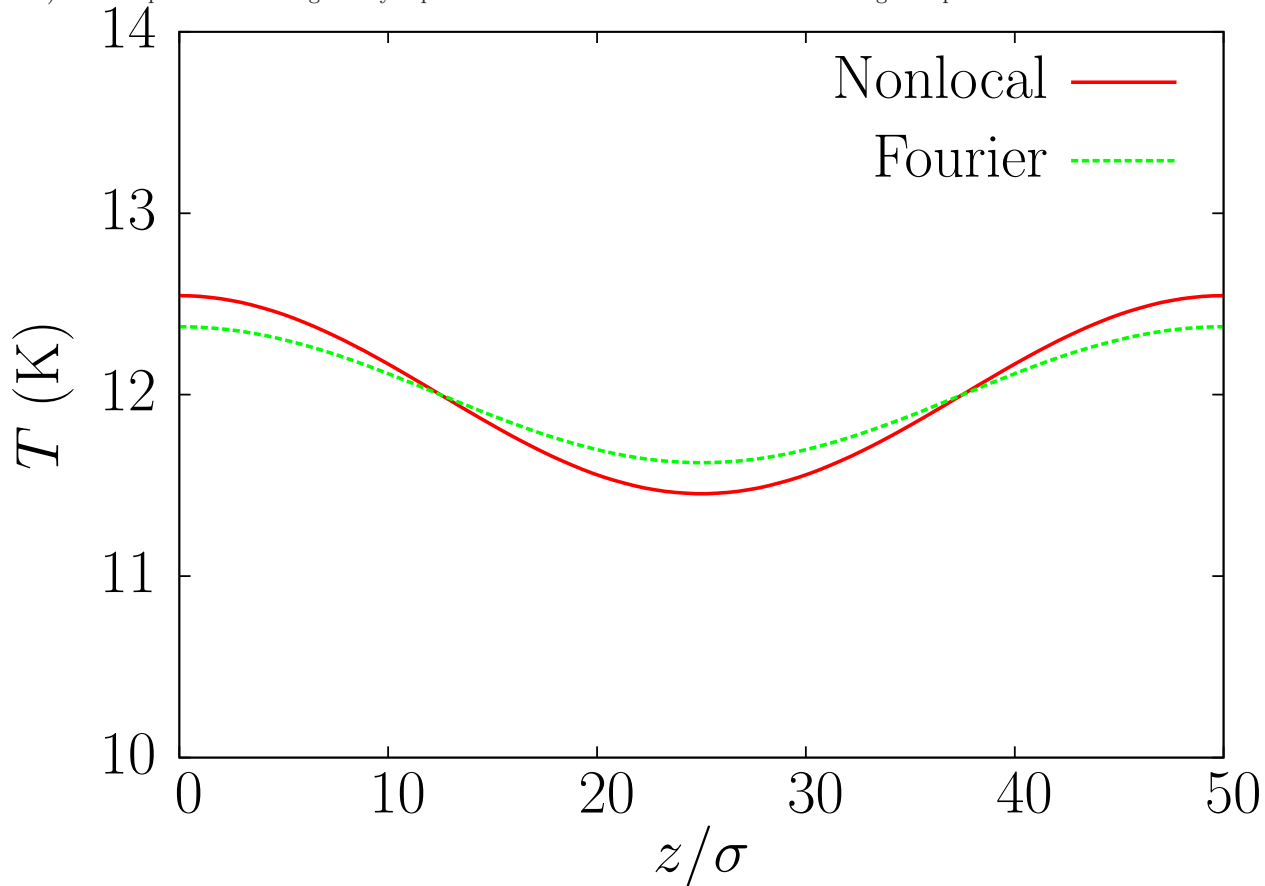


Figure 12: Temperature profiles obtained from the nonlocal response function (solid red line) and Fourier's law (dashed green line) for an input heat source given by Eq. 28. Results shown for time $t = \frac{\pi}{2\omega}$ with average temperature $T = 12\text{K}$.

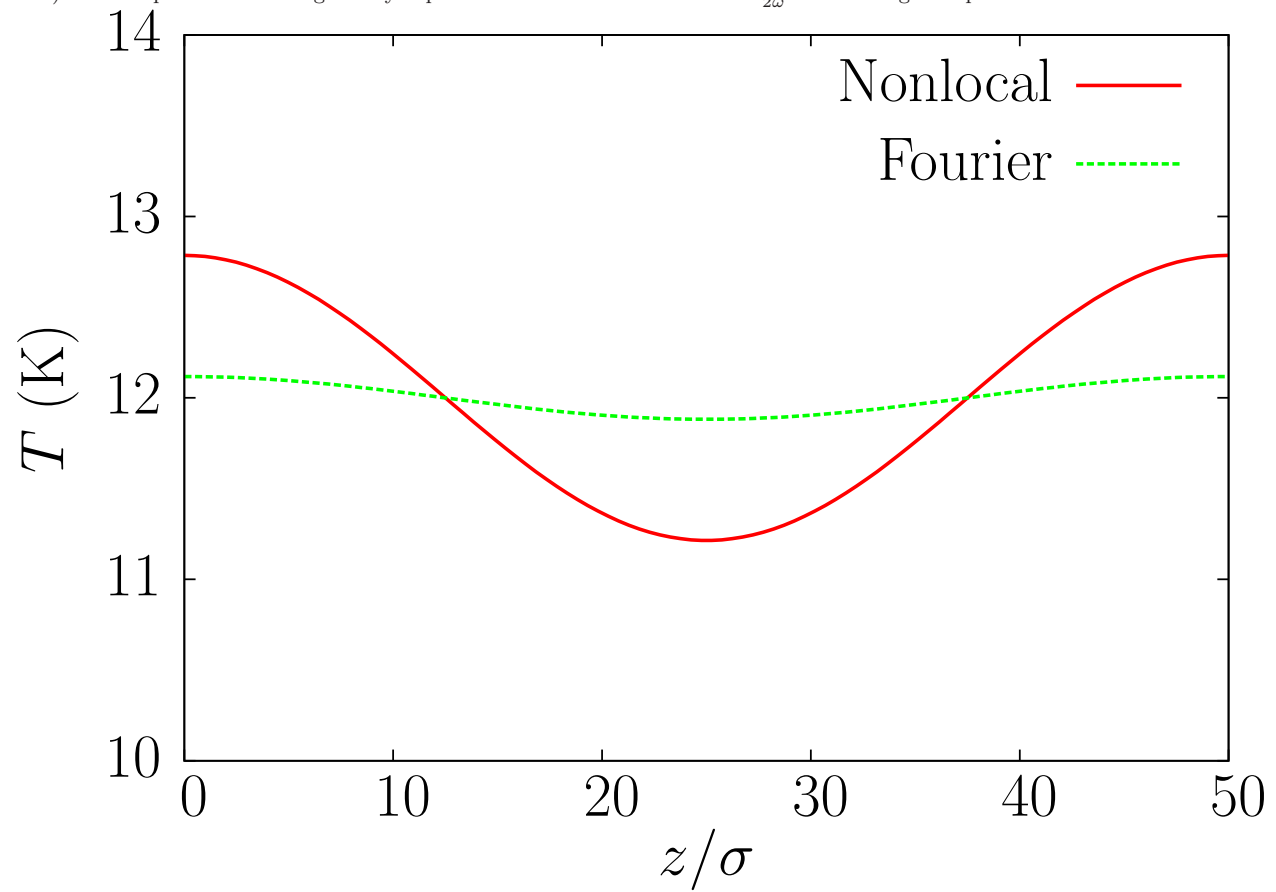


Figure 13: Temperature profiles obtained from the nonlocal response function (solid red line) and Fourier's law (dashed green line) for an input heat source given by Eq. 28. Results shown for time $t = \frac{\pi}{2\omega}$ with average temperature $T = 72\text{K}$.

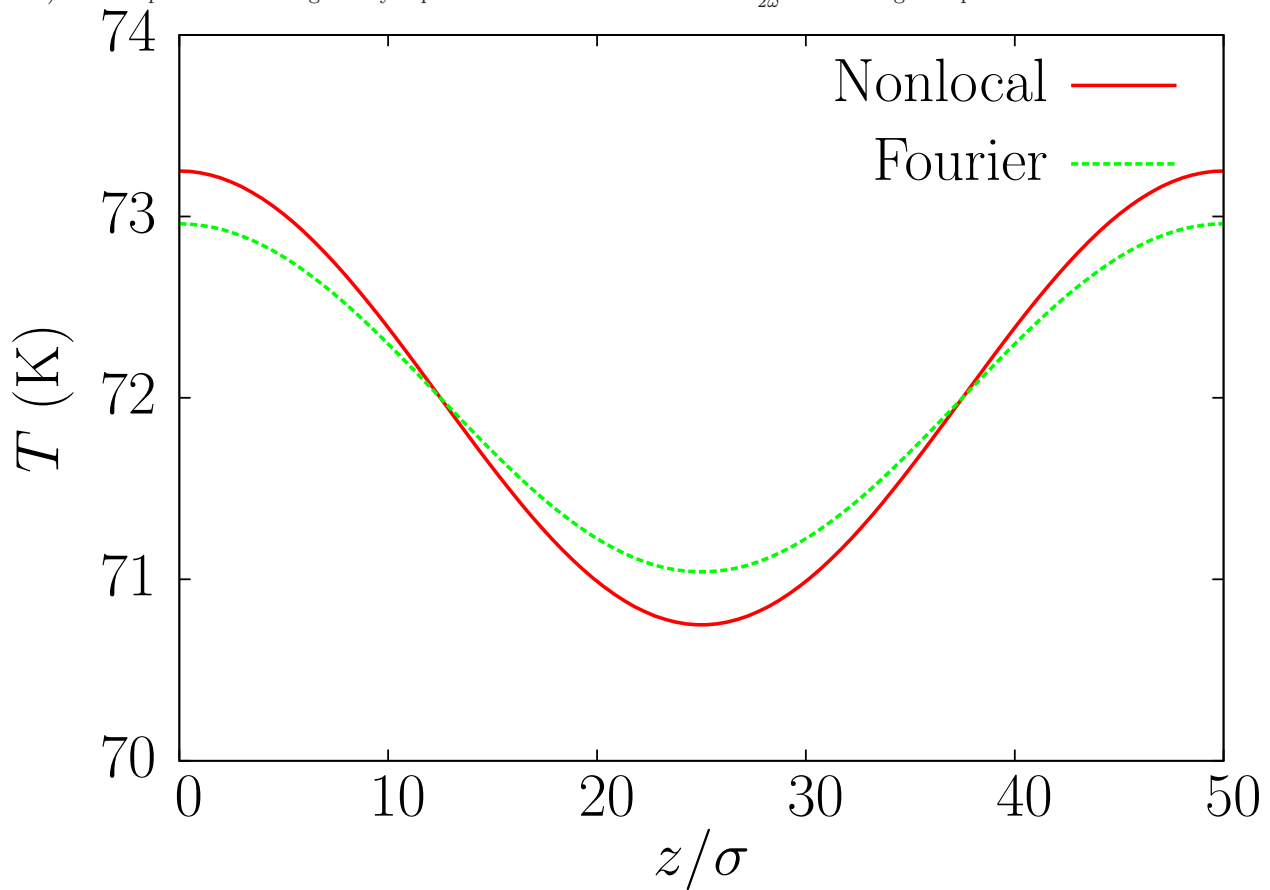


Figure 14: Inverse effective conductivity κ_{eff}^{-1} as a function of inverse length $\frac{k}{2\pi}$ in units σ^{-1} obtained from the nonlocal simulation results and Eq. 37. Values for $k = 0$ obtained from the standard Green-Kubo equation for κ .

